Brønsted-Brønsted Synergies Between Framework and Non-Crystalline Protons in Zeolite H-ZSM-5

Kuizhi Chen,[#] Maryam Abdolrahmani,[♦] Sarah Horstmeier,[♦] Tram N. Pham,[⊗]
Vy T. Nguyen,[⊗] Michael Zeets,[⊗] Bin Wang,[⊗] Steven Crossley,[⊗] and Jeffery L. White[*]

School of Chemical Engineering, Oklahoma State University, Stillwater, OK 74078

Abstract. Zeolite catalysts are solid Brønsted acids whose reactivity is typically associated with the number of protons at crystalline framework bridging acid sites (BAS's). Post-synthetic catalyst modification, titrations with monovalent and divalent cations of varying size, quantitative spin-counting spectroscopy on all protons before and after cation exchange, amine titration, and room-temperature in-situ reactions with two different probe molecules reveal that zeolite HZSM-5 reactivity strongly corresponds with the presence of acidic protons from extra-framework and/or non-crystalline sites. Significantly, room-temperature hydrogen-deuterium (H/D) exchange reactions between the catalyst and organic probe molecules reveal that reaction rates are strongly dependent on the total concentration of acidic protons from extra-framework and non-crystalline proton sites. The most active catalysts in room-temperature probe reactions contain protons from both BAS's and from non-crystalline species, including reactive extra-framework aluminol species that can be removed by solvent treatments. In order to demonstrate the significance of paired framework/extra-framework or non-crystalline Brønsted sites to overall catalyst activity, speciation of different protons were quantified after titration with mono- and divalent cations of varying radius (Na^{+}, Ca^{+2}, Cu^{+2}, Ba^{+2}), chemical washing with ammonium hexafluorosilicate (AHFS), and different steaming procedures for HZSM-5 catalysts with Si/Al equal to 15 and 40. Detailed manipulation of reactive Brønsted species in the Si/Al = 15 catalyst enabled direct experimental observation of H/D exchange at both the methine and methyl positions of isobutane, heretofore not reported, clarifying uncertainties surrounding that

mechanism. Reaction data indicates that isolated framework BAS's are much less important to overall catalyst reactivity than proximate framework/extra-framework or non-crystalline Brønsted sites, and DFT calculations support the importance of proximate proton sites. Potential Brønsted-Brønsted synergies are unique relative to previously proposed Brønsted/Lewis synergies, but does not preclude the latter's contribution to increased reactivity.

* Author to whom all correspondence should be addressed at *jeff.white@okstate.edu*
# Present address National High Magnetic Field Laboratory, Tallahassee, FL
♦Department of Chemistry, Oklahoma State University, Stillwater, OK
⊗School of Chemical, Biological, and Materials Engineering, University of Oklahoma, Norman, OK

Introduction

Zeolite catalysts are widely used industrial catalysts primarily employed in high-temperature conversions of gas-phase reagents,[1-3] but are now increasingly considered for aqueous or biphasic catalysis to transform molecules derived from biomass,[4-7] or as catalysts for environmental remediation.[8-10] The view of acidity in HZSM-5, a member of the MFI structure family, as arising from simple framework bridging acid site models with single-site character[11,12] have recently been demonstrated as too narrow, particularly for catalysts with high aluminum content.[13-17] Recently published reports including variations in synthesis, catalytic testing, computation, and spectroscopic investigations indicate that different Al sites in the catalyst framework exist, and that the details of Al siting, e.g. at channel intersections or in straight channels, can be critical to catalyst performance.[18-22] At high Al concentrations in the framework, inter-site proximity can in theory introduce synergistic contributions that increase catalyst activity, either through transition-state stabilization, increased adsorption, or via enhanced proton conductivity.[23-25] Experimental efforts to quantify the number of proximate or "paired" sites through divalent cation titration have been reported.[22,25] Differential catalyst reactivity in high- versus low-Al HZSM-5 has also been attributed to increased populations of Al at bridging acid sites (BAS) in the straight channels relative to channel intersection sites.[16] In subsequently published studies, residual extra-framework Al (EFAl) sites can remain in HZSM-5 following washing with common reagents like EDTA, and those sites have been shown to significantly contribute to Brønsted acidity.[26] Al siting studies using MQMAS NMR experiments reveal multiple potential T-sites for Al, as would be expected based on the known crystallographically inequivalent sites in MFI structure.[27-29] More interesting is the differential relative stability of those sites in channel intersections versus straight channels, and many

recently published studies suggests differences in the reactivity of those sites as listed in the above references. Al-atom siting in crystalline T-sites is an important topic of current interest; Al in some extra-framework sites or in partially-coordinated framework sites[18,30-32]could lead to active Brønsted sites or impact existing sites, and therefore it is critical to directly probe Brønsted proton site distributions in HZSM-5 and related catalysts.

In this contribution, Brønsted proton siting in HZSM-5 catalysts with different Si/Al's is examined through a combination of post-synthetic cation titrations and chemical washing, in-situ probe molecule reactivity, steaming, and direct spectroscopic inspection of the Brønsted proton active sites. Quantitative spin-counting NMR results on HZSM-5 catalysts with Si/Al ratios of 15 and 40, before and after titrating with monovalent and divalent cations and/or washing with AHFS (ammonium hexafluorosilicate) reveal that while proximate Brønsted sites within the framework do exist and increase with decreasing Si/Al as expected, Brønsted proton sites from defect site species are required for maximum activity. In addition to including acidic EFAl protons or protons from non-crystalline regions similar to amorphous silica-alumina, the term non-crystalline proton site is used here to also include aluminols that may be partially framework bound. In this latter case, such sites experience large deviations from the normal tetrahedral framework geometry, and their Al signals are not observable in dry zeolites, but their associated Brønsted acid proton can be detected. Cation titrations show that some of the defect Brønsted sites are proximate to framework BAS, indicating that Brønsted-Brønsted synergy between BAS and defect Brønsted sites can contribute to overall acidity. The fraction of total Brønsted protons, arising both from BAS and EFAl sites, which are eliminated by divalent cation exchange in the two Si/Al ratio catalysts (15 and 40) depends on the cation and the exchange method. Attempts to confidently interpret literature reports where divalent cation titration is

used to quantify "paired" acid sites can be problematic due to variable exchange conditions and the fact that some reports use only single cation exchange steps, thereby preventing complete site exchange. Using large cations like Ba^{2+} with atomic dimensions closer to that of the critical diameter of small hydrocarbon reagents shows that Brønsted protons from defect species exist in close proximity to framework BAS's. As introduced here, cation titrations coupled with ^{1}H MAS NMR provide advantages over traditional approaches in which UV-Vis spectroscopic detection requires the use of only certain cations, e.g., Cu^{2+} or Co^{2+}, thereby increasing the range of cation size available. In addition, this experimental approach also ensures that the cations actually displace acidic protons at active sites versus simple adsorption on the surface, and quantifies that exchange.

When acidic non-crystalline and/or EFAl hydroxyls (i.e., aluminols) are present along with framework BAS's, reaction rates for room-temperature H/D exchange between either an alkane or aromatic probe molecule and the catalyst are maximum. When the EFAl species are removed using known chemical washing methods, reaction rates decrease dramatically. Following their removal, or starting from high Si/Al catalysts without such species, the Brønsted protons from these aluminol species can be re-introduced to the catalyst by steaming as shown by direct NMR observation, with concomitant increase in reaction rates even for the Si/Al=40 catalyst consistent with the migration of those aluminols near framework sites. Reaction rate constants for benzene H/D exchange are a strong function of the concentration of proximate framework/extra-framework/non-crystalline Brønsted acid sites. In total, this contribution helps address several key questions in the current literature, including the role of paired active sites in high-Al content zeotype catalysts, types of "defect" Brønsted sites, contributions to acid-

catalyzed chemistry from minor acid site populations, and synergistic contributions from water in the presence of defect acid sites.

Experimental

Catalyst samples. Zeolite ZSM-5 samples with different aluminum content (Si/Al = 15 CBV 3024E and Si/Al= 40 CBV 8014) were obtained from Zeolyst in the ammonium-exchanged form**.** The BET surface areas vary from 379-386 m^2/g independent of Si/Al ratios,[33] and SEM experiments indicated that the average particle size was 0.6-0.7 μm. Dehydrated HZSM-5 zeolite samples were prepared from the ammonium form in a glass reactor body via a stepwise vacuum procedure to a final temperature of 723 K, under 2×10^{-5} torr using an Edwards EO4K diffusion pump. To ensure all water was removed, as indicated by increased T_1 values for the catalyst protons,[15] some samples were dehydrated using a flow reactor with ultrapure argon or helium gas, heated stepwise to a final temperature of 723-773 K, and held there for 24 h. In some cases, denoted as AHFS-washed, as-received Si/Al = 15 catalysts in the ammonium form were washed with ammonium hexafluorosilicate (AHFS) using standard methods.[34,35] Catalysts were dispersed in deionized water at a concentration of 30 g/L, corresponding to an AHFS:Al ratio of 2. The mixture was heated to 90 ^{o}C under vigorous agitation. 5 ml of 0.4 M of AHFS solution was added very slowly to the mixture. After 4 hours stirring, the final mixture was filtered and washed three times with the hot deionized water, followed by vacuum stepwise dehydration in the same way as the unwashed HZSM-5 samples. To prepare "mild-steamed" catalysts, the washed sample was further treated by steaming with 21 Torr water vapor in nitrogen flow at 12 mL/min in a flow reactor, heated stepwise (0.63 ^{o}C/min up to 100 ^{o}C, held at 100 ^{o}C for one hour) to a final temperature of 500 °C, and held there for 72 h. There was no liquid water present at any time. After steaming, the samples were dehydrated using the flow reactor with

nitrogen gas at 500 °C for 5 h. For "severe steaming", the procedure was same as the mild steaming method, but the washed sample was steamed at 600 °C for 72 h. After steaming, the samples were dehydrated using the flow reactor with nitrogen gas at 500 °C for 5 h. No reactions were done on the severely-steamed catalysts.

Divalent cation exchange experiments employed cations varying in size, including Na^{+}, Ca^{2+}, Cu^{2+}, and Ba^{2+}. The ion-exchanged form of each zeolite was prepared by treating 80 mg of the H^{+} form with 4 ml of either 0.1 M aqueous $Cu(NO_3)_2$, $Ca(NO_3)_2$, $Ba(NO_3)_2$, or $NaNO_3$ at 70 ˚C under stirring in a test tube. After 6 h, the mixture was centrifuged and the supernatant was discarded. These steps were repeated twice, for a total of three exchange cycles, to ensure complete removal of exchangeable protons. Additional exchange steps produced no change in the spectra. Centrifugation, versus filtration, minimizes catalyst loss during multistep treatments and essentially 100% of the catalyst by mass was recovered after multiple treatments. After a total of three exchanges and separations, the last solid isolate was added to 4 ml of deionized water, stirred at 70 ˚C for 6 h, centrifuged, and washed with deionized water 3 times at room temperature. This procedure was repeated twice with the total of 3 washes at 70 ˚C and 9 washes at room temperature, to completely remove excess physisorbed cations. After all the treatments above, 70-80 mg of ion-exchanged catalyst was recovered and dehydrated under vacuum for further use.

Benzene-d_6 and isobutane-d_{10} H/D exchange experiments with HZSM-5. A vacuum line equipped with a CAVERN type apparatus was used for quantitative adsorption, following previously published procedures.[36,37] A fixed quantity of catalyst was placed in a 4-mm zirconia MAS NMR rotor in the CAVERN, evacuated and sealed. The isobutane-d_{10} (> 99.1%, CDN Isotopes) or benzene-d_6 gas (99.6% purity, SigmaAldrich) was then introduced in the vacuum

line to an initial pressure. The adsorption was stopped at a calculated final pressure corresponding to a 1:1 ratio of hydrocarbon:acid site, i.e., 1 equivalent (eqv). H/D isotopic exchange took place immediately after adsorptions, while the adsorption processes usually took 3 minutes for completion. The initial H/D exchange spectra were typically acquired 5-10 minutes following the initial exposure, but given the relatively small exchange rates at room temperature, initial rates are easily linearly extrapolated back to time zero as discussed below. Given the large reduction in crystallinity for the severe-steamed catalysts (Table S1) and accompanying reduction of acid site density (see Table 1, Figure 1), the severe-steamed catalysts were not used for reactivity comparisons.

Solid-state NMR spectroscopy. ^{1}H MAS (magic-angle spinning) NMR data was collected on a Bruker Avance 400 spectrometer operating at 9.05 T with a 4-mm double-resonance MAS probe. When necessary, as mentioned in the text, the rotors were spun with dry nitrogen gas to avoid possibility of moisture contamination following sample sealing. Spinning speeds of 10 or 15 kHz, 32 scans and 3.9 μs $\pi/2$ excitation pulse were used for single-pulse acquisitions. Recycle delays of 60 s were used for quantitative experiments on dry catalysts, but in the range of 2-5 s for rate measurements in order to follow the reaction on an appropriate timescale. Given the small signal-averaging time for the single-pulse ^{1}H MAS experiments, an empty rotor probe background spectrum was acquired separately for each run and subtracted from the zeolite spectrum in order to remove a small background signal near 1 ppm. ^{1}H spin-lattice relaxation time constants T_1 was measured using a modified saturation recovery pulse sequence in which the 90˚-read pulse was replaced by a composite 90˚ pulse as previously described by Cory,[38] and data were acquired with 10-kHz MAS speeds.

Isopropylamine TPD measurements. Temperature programmed desorption (TPD) of adsorbed isopropylamine (IPA) was applied to determine the density of Brønsted acid sites for the initial and washed HZSM-5, providing a complementary measure of BAS concentration to the NMR in terms of probe-molecule accessibility. The pelletized catalyst mixed with glass beads was utilized in each TPD experiment which has the same condition as catalyst used for tested reactions. The pretreatment was conducted at 300^{o}C for 2 h, then the catalyst was cooled to 100^{o}C under 30 ml/min of He and exposed to several 2 μL pulses of IPA. After flushing the catalyst under He for 4 h at 100^{o}C to remove weakly adsorbed IPA, a 10 ^{o}C/min linear heating ramp was applied up to 550^{o}C. The analysis was done using MKS Cirrus 200 quadrupole mass spectrometer (MS), tracking m/z = 58, 41, 17 for IPA, propylene and ammonia respectively. The propylene signal (m/z = 41) was calibrated with 500 μL propylene pulses. Raw data are shown in Figure S2 of the Supporting Information.

Surface area and nitrogen adsorption measurements. BET surface areas were determined for HZSM-5 (Si/Al=15) and the same HZSM-5 treated with AHFS (AHFS:Al = 2:1) at liquid nitrogen temperature using a Quantachrome Autosorb-1 instrument. Each sample was degassed at 423 K overnight prior to nitrogen adsorption. For the as-received HZSM-5, the BET surface area was 352 m^2/g, versus 315 m^2/g for the AHFS-washed catalyst.

Crystallinity and elemental analysis. XRD was used to calculate the HZSM-5 crystallinity following some post-synthetic chemical treatments using a Philips PW 1830 diffractometer operating with a Cu Kα radiation (λ = 1.5418 Å) source. Data was gathered in the 5−70° 2θ range with step width set to 0.02° and scanning speed at 0.5 sec/step. Al and Si contents were determined via standard ICP-AES methods from Galbraith Laboratories.

Cracking activity measurements. n-Hexane cracking over the initial and washed HZSM-5 catalysts (Si/Al = 15) was evaluated on a micropulse reactor in He carrier gas (atmospheric pressure). 5 mg of each catalyst pelletized to 0.25-0.35 mm particles, then mixed with 95 mg of glass beads, was utilized for the reaction. The temperature of the reaction is 480 $^{\circ}$C. Before reaction, the catalyst was pretreated under the reaction temperature for 1h. After pretreatment, several pulses of the hydrocarbon reactant diluted in He (0.48 μmol HC/pulse, 3.7 mol% of HC in He) were sent over the catalyst bed with 75 ml/min He flow. During the 1h period between pulses, the catalyst was exposed to continuous flow of He. The products of the reaction were analyzed online by an Shimadzu QP-2010 GCMS/FID system equipped with an HP-PLOT/Al_2O_3/''S'' column which is directly connected to the reactor outlet. The reactions were stopped after 3 pulses as the results at subsequent pulses were similar.

DFT Calculations. All density functional theory (DFT) calculations were performed using the Vienna ab-initio simulation package (VASP)[1] with the projector augmented wave (PAW) method.[39,40] The PBE generalized gradient approximation (GGA) exchange-correlation potential was used.[41] The van der Waals interaction was included through DFT-D3 semi-empirical methods via a pairwise force field.[42,43] The structural relaxation was carried out with plane-wave kinetic cutoff energy at 400 eV. All atoms in the zeolite unit cell were fully relaxed and the convergence criterion for the atomic net force on atoms was 0.02 eV Å^{-1}. The unit cell of H-ZSM-5 was used in all calculations. The structure was composed of 96 T atoms (T = Si, Al) and 192 oxygen atoms. The lattice constants of MFI unit cell were set to a = 20.078 Å, b = 19.894 Å, c = 13.372 Å, which were taken from experimental work.[44] Among the 96 T sites, there are 12 geometrically distinguishable T site locations that can be occupied by Al. To calculate the chemical shift of EFAL, an EFAl was fixed at the T7 site, which is shown to have high

stability.[45,46] That is, one framework Al was fixed at T7 to balance the charge of EFAL. The chemical shift of protons was calculated using the linear response function method.[47,48]

Results and Discussion

The key benefit in using ^{1}H solid-state NMR to interrogate protonic species in zeolites is that it provides a direct, quantitative signal from all species including Brønsted acid site protons.[49-51] ^{1}H solid-state NMR does not suffer from the limitations of ambiguous extinction coefficient and scattering effects associated with infrared spectroscopy of powders, and has been recently discussed in the literature as a way to calibrate the latter.[52] Figure 1 shows high-resolution ^{1}H MAS NMR spectra for HZSM-5 catalysts in their dry, protonic form, i.e., in the absence of atmospheric exposure. Peaks are labeled according to previously reported assignments,[15,26] with 1a-d and 1e corresponding to Si/Al=15 and 40, respectively. The two largest peaks in each of the spectra, excluding the spectrum in 1d, correspond to the well-known crystalline BAS's (4.2 ppm) in the framework and the silanol hydroxyl groups (1.8-2 ppm) at crystallite termini. In comparing the bottom spectrum in 1a, corresponding to as-prepared Si/Al = 15, to the spectrum in 1e for the similar Si/Al=40, the relative intensity of these two peaks are reversed due to the much lower BAS density in the latter, as expected. The main purpose in showing the data in Figure 1, however, is to demonstrate the populations of additional protonic species whose identity and function are less well understood, indicated by the relatively narrow peak at 2.8 ppm, and the broad peaks from ca. 5-7 ppm and 12-15 ppm. These peaks can be easily deconvoluted from the rest of the spectrum, as shown by the dashed lines in Figure 1a. For clarity, they are not shown in 1b-1e. Previously, the 2.6 and recently-discovered 12-15 ppm peaks were assigned to hydroxyl groups from EFAl species (H-EFAl), as they are easily removed by chemical washing.[15] The broad shoulder slightly downfield of the BAS peak, visible

from 5-7 ppm, has been recently assigned as arising from a combination of EFAl hydroxyl species and framework acid sites with uniquely distorted or coupled bonding environments,[15,26] the latter of which was originally proposed in 1994.[53] Previously, the 5-7 ppm region was also assigned to framework BAS's that were hydrogen bonded,[50] not inconsistent with our assignments as discussed in more detail below. The assignment of the protons giving rise to the intensity in the 5-7 ppm region, which is a significant fraction of the total proton intensity, continues to be debated in the literature, with some relatively recent reports claiming it as residual water.[54] Recent quantitative spin-counting analysis of several HZSM-5 catalysts eliminated the possibility that this peak arises primarily from residual water.[26] Figure 1a shows that the deconvoluted 5-7 ppm peak requires at least two components to accurately fit, which will be discussed in more detail later in the contribution. With the exception of the SiOH terminal silanol species represented by the 1.8-2 ppm peak in Figure 1, all other species have been recently shown to act as Brønsted acid sites in room-temperature H/D exchange reactions with a hydrocarbon reagent.[15]

Note that the distribution of species is very different in 1a and 1e for the as-synthesized Si/Al = 15 and Si/Al = 40 catalysts, respectively. In addition, within the series of spectra for the former, the relative contribution of each of the species varies dramatically with sample history. To be clear, there are at least five different types of protons as indicated by the five different peaks in 1a-d. In going from 1a to 1b, the as-received commercial catalyst following slow, stepwise vacuum dehydration (1a) was washed using ammonium hexafluorosilicate (AHFS) (1b), yielding a spectrum devoid of the H-EFAl groups giving rise to the 2.8 and 12-15 ppm peaks. However, figure 1c shows that these species can be reintroduced following the mild steaming procedure defined in the Experimental section, since both the 2.8 and 12-15 peaks

reappear, while still preserving most of the BAS's as indicated by the 4.2 ppm signal. Similar behavior is seen for the Si/Al = 40 catalyst in 1e, which does not have any detectable H-EFAl species in the initial catalyst. Following mild steaming, however, small contributions from the species giving rise to the 2.8 and 12-15 ppm peaks can be observed in the red overlay spectrum in 1e, with concomitant decrease in the framework BAS signal intensity. Finally, Figure 1d shows that severe steaming eliminates almost all BAS's, and in addition to the previously discussed H-EFAl species, generates additional non-crystalline protons indicated by the 1-ppm signal that is not observed in other catalysts. Table S1 shows crystallinity data for all catalysts.

The result in 1e indicates that even in the relatively low-Al content HZSM-5, which has no detectable sites in the ^{1}H NMR other than framework BAS's, the H-EFAl species can be introduced by appropriate treatment. While the amounts of the 12-15 and 2.8 ppm peaks shown in the red spectrum of 1e appear very small, their impact is significant. Using isobutane-d_{10} as a probe reagent for room-temperature reactivity, rate constants for the H/D exchange reaction between this saturated hydrocarbon and the Si/Al = 40 HZSM-5 were measured for the two samples shown in Figure 1e. The as-prepared catalyst (black trace in 1e) yielded an exchange rate constant $\mathbf{k_{ex} \leq 1.7\times10^{-6}\ s^{-1}}$, whereas the mild-steamed catalyst (red trace in 1e) was characterized by a rate constant $\mathbf{k_{ex} = 1.5\times10^{-5}\ s^{-1}}$. The steamed catalyst in 1e has a much lower BAS concentration than the initial catalyst, but an order of magnitude increase in the rate constant for the H/D exchange reaction due to the generation of H-EFAl species giving rise to the 12-15 and the 2.8 ppm peaks that were not present in the original catalyst. The amounts of all species can be quantified using the spin-counting standard-addition method,[55] in which a known amount of an inert PDMS (polydimethylsiloxane) in the solid state is added to the rotor with the catalyst, as shown by the presence of the intense peak at 0 ppm in the steamed spectrum

in Figure 1e. Using this method, the BAS concentration in the steamed Si/Al = 40 catalyst in Figure 1e decreases by a factor of 5 compared to the initial catalyst, and yet the reaction rate increases by a factor of 10. Given that the details of the spin-counting method have been previously published,[26,55] the raw spin-counting solid-state NMR data for each of the other samples shown in Figure 1 (1a-d) are provided for convenience in Figure S1, yielding quantitative population distributions for each proton type (*vide infra*). For convenience, the accompanying ^{27}Al MAS NMR spectra are also shown in Figure S1 for the same samples in their hydrated forms, i.e., exposed to ambient moisture.

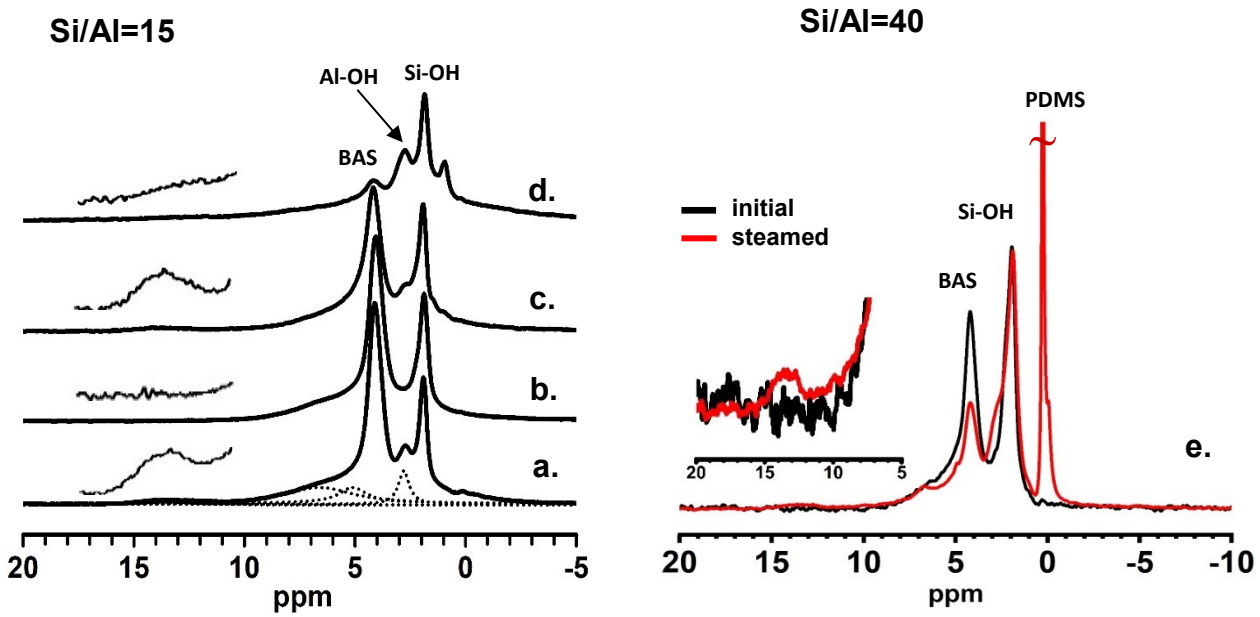

Figure 1. ^{1}H MAS NMR spectra of **(a)** as-prepared HZSM-5 with Si/Al = 15 following step-wise vacuum dehydration; **(b)** same as (a) treated with AHFS:Al = 2; **(c)** same as (b) following a mild steaming procedure; **(d)** same as (b) following the severe-steaming procedure; **(e)** Si/Al = 40, with the as-prepared catalyst shown in black and the mild-steamed catalyst shown in red along with the PDMS intensity standard. The PDMS peak in 1e is artificially attenuated in the figure for clarity. The insets show signal originating from elimination and creation of acidic H-EFAl species (12−15 ppm region).

To further explore the connection between the distribution of acidic protons in HZSM-5 and reactivity revealed by the data in Figure 1e, benzene-d_6 was used as a reactivity probe for each of the catalysts shown in Figure 1. From quantitative spin-counting experiments, concentrations of each protonic component for the four Si/Al = 15 catalysts were calculated and are listed in Table 1 below. Examination of the information summarized in the last three columns of Table 1 is revealing. The total concentration of all non-SiOH (i.e., excluding silanol groups) protonic species in the initial HZSM-5 catalyst is 1.1 mmol/g, very near the expected value of 1.04 mmol/g based on total Al content. As expected, this total decreases with subsequent treatments, due to the combined effects of extraction of H-EFAl species with AHFS and condensation/dihydroxylation associated with the steaming steps. The very small increase in SiOH (first column) with subsequent steps is trivial compared to the loss of all other species, and in particular to the almost order of magnitude decrease in the BAS concentration. Comparing the data in the last two columns, which lists the concentration of framework BAS's and protonic species arising from EFAl and/or non-crystalline species (i.e., the sum of 2.8, 5-7, 12-15, and 1 ppm peaks), to reaction rate constants for the benzene H/D exchange reaction on each catalysts yields surprising results. Figure 2 shows a representative example of ^{1}H MAS exchange NMR spectra for benzene on each of the four HZSM-5 catalysts listed in Table 1, at a single time point. The H/D exchange rate is then extracted via the rate of growth of the resolved benzene signal near 7 ppm over the entire time range, from immediately after benzene adsorption to several hours, as has been previously discussed.[37]

Table 1. Distribution of species, in units of **mmol/g**, obtained from quantitative ^{1}H MAS NMR spin-counting spectra of the HZSM-5 Si/Al = 15 catalysts shown in Figure 1. The raw spin-counting spectra and total deconvoluted fits are shown in Figure S1, and are processed according to the previously described method.[26] (*: expected sum for H:Al = 1 is 1.04 mmol/g based on Zeolyst specifications, or 0.90 mmol/g based on Al elemental analysis data from Galbraith Laboratories).

Catalyst	**SiOH** 1.9 ppm	**H-EFAl** 2.8ppm	**H-EFAl/non-xtal** 5-7ppm	**H-EFAl** 12-15ppm	**H-EFAl** 1 ppm	**sum of all species except SiOH**	**BAS** 4.2 ppm	**Sum of H-EFAl/non-xtal species**
Initial	0.18 ±0.01	0.09 ±0.01	0.45±0.037	0.059 ±0.0.025	0	1.1*	0.56±0.018	0.59
AHFS-washed	0.20 ±0.01	0.030 ±0.003	0.28±0.019	0	0	0.84	0.54±0.020	0.31
mild-steamed	0.20	0.080	0.32	0.021	0	0.80	0.38	0.42
severe-steamed	0.21	0.17	0.25	0.018	0.029	0.53	0.064	0.46

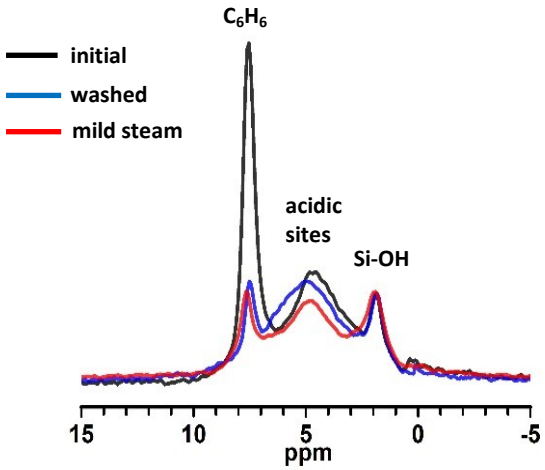

Figure 2. Representative benzene/catalyst H/D exchange spectra acquired 8 minutes after adsorption of benzene-d_6 on Si/Al = 15 HZSM-5, as listed in Table 1 and indicated by the legend. These spectra are a single time point out of many to illustrate how the raw data appear.

The raw data for the benzene exchange rates are shown in Figure 3, in which the rate of growth of the benzene signal (ca. 7 ppm) arising from catalyst protonation is shown versus time for the same three catalysts shown in Figure 2. The signal intensity on the y-axis is given in arbitrary units. Rates are extracted via an initial-growth approximation to the linear region of the

growth curve, as shown by the dotted lines, and are reported along with [BAS] in the figure legend. Clearly, the initial HZSM-5 catalyst is most active, and the signal growth curve fits well to the expected first order $I(t) = I(\infty)[1- e^{(-kt)}]$ function, where $I(\infty)$ represents the equilibrium signal intensity at long exchange time. Due to experimental limitations, it is difficult to acquire data points earlier than 7 or 8 minutes, but control experiments in which benzene-d_6 is adsorbed onto a non-acidic silica show that there is no proton signal intensity arising from impurities in the benzene, thereby validating the assumption that the signal intensity at time zero is zero and that the fit curve should go through the origin, as it does. Since the benzene signal increases over an order of magnitude slower for the washed and mild-steamed samples, the initial rate is determined by a linear least squares fit through the data points as shown by the two dashed lines at the bottom of Figure 3. Comparing the exchange rates from the initial rate approximation along with the BAS concentration in Figure 3 for each catalyst reveals that the exchange rate does not depend on BAS concentration, but appears to strongly depend on the concentration of acidic protons arising from defect species listed in Table 1. Again, the latter are identified by the signals in Figure 1a-1d in the 2.8, 5-7, and 12-15 ppm regions. Since the NMR signal intensity units are arbitrary (denoted a.u.), the reported rates are normalized to the smallest initial slope value, i.e., the washed HZSM-5, at R=1 $(a.u.)\cdot s^{-1}$. The exchange rate for the initial HZSM-5, which has essentially the same [BAS], is R=23 $(a.u.)\cdot s^{-1}$. Finally, the mild-steamed catalyst is characterized by an exchange rate R = 1.9 $(a.u.)\cdot s^{-1}$. Thus, even though the initial and washed HZSM-5 catalysts have the same concentration of framework bridging acid sites, there is a ca. 20-fold difference in their reaction rates as determined via an initial-rate analysis of the slope of the line fit to a first-order model. The benzene exchange data on the initial HZSM-5

catalyst was collected out to a reaction time of 90 minutes, which is shown along with the fitting curve in Figure S3 for reference to further validate the fitting out to long reaction times.

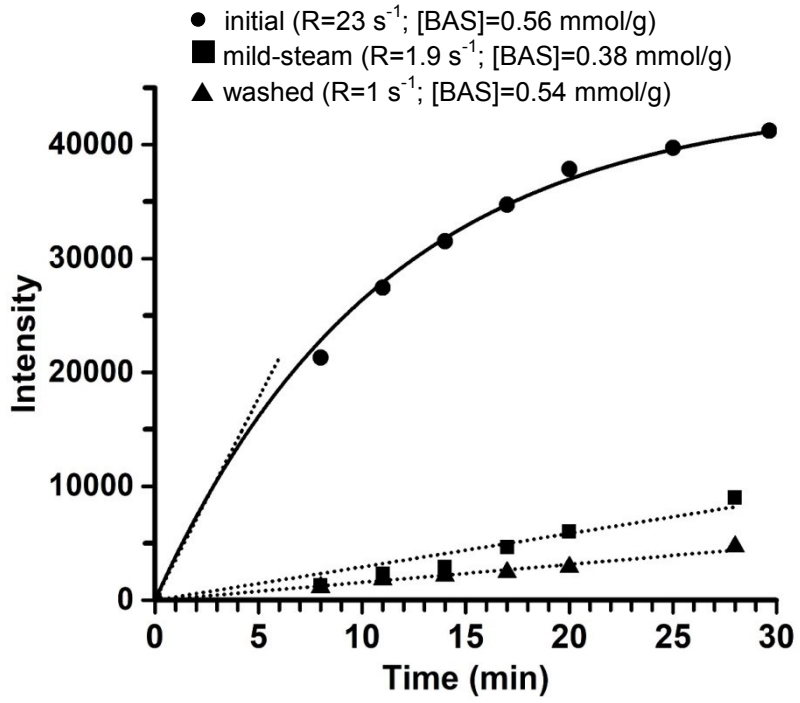

Figure 3. Raw data for the benzene signal intensity versus reaction time for room temperature benzene-d_6 H/D exchange experiments in three of the catalysts detailed in Table 1. The exchange rates R and the BAS concentration [BAS] are noted in the legend with rates normalized to that of the washed HZSM-5. The solid line is the fit of the initial catalyst/benzene data to the first order rate model given by $I(t) = I(\infty)[1- e^{(-kt)}]$. Fits of the initial catalyst curve out to 90 minutes are shown in Figure S3.

n-Hexane cracking measurements and IPA TPD results. As a complement to the room-temperature H/D exchange data discussed above, n-hexane cracking experiments were carried out at 480°C in a pulsed microreactor for the initial and AHFS-washed HZSM-5 catalysts. Prior to reaction, IPA TPD measurements (Figure S2) revealed that the total concentration of Brønsted acid sites was 0.76 and 0.74 mmol/g for the initial versus washed HZSM-5, respectively. This agrees with the NMR data in Table 1, in that the AHFS washing does not remove framework

BAS's. The fact that the total Brønsted acid site amount equal 0.76 mmol/g measured by IPA TPD exceeds the 0.56 mmol/g, reported in Table 1 by following the traditional assignment of the 4.2 ppm peak to crystalline BAS proton species, is suggestive that other Brønsted acid sites are giving rise to the residual intensity (0.28 mmol/g) in the 5-7 ppm region following AHFS washing. Under identical reaction conditions, n-hexane conversion was 2% per unit catalyst mass for the initial HZSM-5, but only 0.6% for the washed catalyst. Thus, the trends in catalyst activity indicated by the room-temperature probe-reaction data in Figures 2 and 3, attributed to proximate crystalline framework and non-crystalline acid sites, are likely important in more typical high-temperature reactions involving carbon-carbon bond breaking.

Importance of proximate framework and non-crystalline Brønsted sites. The initial, as-prepared catalyst has the highest concentration of BAS and protonic species from EFAl and non-crystalline regions, and as expected, exhibits the largest reaction rates in Figure 3. However, examination of the data in Table 1 and Figure 3 shows that the relationship between reaction rate and concentration of BAS or non-BAS acidic protons is not linear. For example, the AHFS-washed sample has almost the same [BAS] as the parent zeolite, and ca. 60% of non-BAS acidic protons, but the lowest reaction rate among all catalyst. From Figure 1, it is clear that the washed catalyst has no 12-15 ppm or 2.8 ppm species. (If residual AHFS was present following the treatment of the initial catalyst, acting to block pores in the washed sample, then new, relatively sharp signals in the ^{1}H NMR spectrum would be observed arising from the ammonium cation; no such signals are observed. Indeed, signals are lost, not gained, as discussed extensively above.) Benzene has a larger proton affinity (180 kcal/mole) than water (165 kcal/mole), and indeed is significantly larger than the proton affinity of isobutane (162 kcal/mole) used to obtain similar increased reactivity with increased non-BAS content shown in 1e. One could argue that

the increase in amount of H-EFAl/non-crystalline species that coincided with increased isobutane reactivity in 1e could be explained by a simultaneous Lewis/Brønsted synergy arising from EFAl species and framework BASs, or from Lewis sites initiating isobutane H/D exchange via hydride abstraction. Given its large proton affinity, it is not reasonable that the initiation step for benzene H/D exchange would include hydride abstraction. This is supported by recently published mechanism for benzene activation via protonation, in which it was shown that benzene/catalyst H/D exchange reactions are good probes for zeolite catalyst acidity.[56] The impact of acidic proton distributions in the four catalysts detailed in Table 1 on the reaction rates in Figure 3 is significant, and cannot simply be explained based on maximum amounts of either type (BAS versus non-BAS) of acid site, nor based on BAS proximity or paired-framework sites, since the Si/Al = 15 catalyst after AHFS washing still has the same framework BAS content. This is confirmed even in the much lower acid density Si/Al=40 catalyst based on the results in Figure 1e. What is apparent from the data is that ***both BAS's and acidic protons from EFAl and non-crystalline sites, i.e., defect sites,*** must be present for maximum reactivity, suggesting that a framework BAS/defect site Brønsted-Brønsted acid site synergy can be important for zeolite reactivity.

Computational evidence for proximate framework and non-crystalline acid sites. MFI structures were generated using DFT methods (VASP/PAW) detailed in the Experimental section. Figure 4 shows results for the case of both an isolated Brønsted site (4a), and a paired-framework, i.e., next nearest neighbor Al atoms, Brønsted site (4b). In each case, a logical aluminol species is added based on charge-balance needs. For the isolated BAS, the framework Brønsted proton is proximate to an $Al(OH)_3$ species (4a), while for the paired site, the relevant aluminol species is $Al(OH)_2^+$ (4b). Calculated ^1H chemical shifts are shown next to each proton

species; for reference, the calculated structure and chemical shift for an isolated BAS (T7 site) is given in Figure S4 of the Supporting Information. The 4.4 ppm value calculated and shown in Figure S4 is in agreement with the known 4.2 ppm peak for the BAS shown in Figure 1. Figure 4a and 4b demonstrate that large downfield shifts in the framework BAS signal to regions near 15 ppm are induced by proximate EFAl species, which is in agreement with the broad 13-15 ppm signal shown in Figure 1a, c, and e. In addition, Figure 4a shows that contributions to the broad signal in the 5-7 ppm regions discussed above can arise from a proximate non-crystalline hydroxyl group on an EFAl species, shown at 6.6 ppm in the calculated structure. Doubtless there is a distribution of species, but clearly the signals associated with their presence as shown in the DFT calculation disappear after AHFS-washing, as shown in Figure 1b. In addition, the chemical structure of the aluminol species shown in Figure 4 may likely change at higher temperatures, e.g., of the type relevant to the n-hexane cracking rates discussed above, due to further dihydroxylation, at which point a Brønsted-Lewis synergy could become the dominant effect.

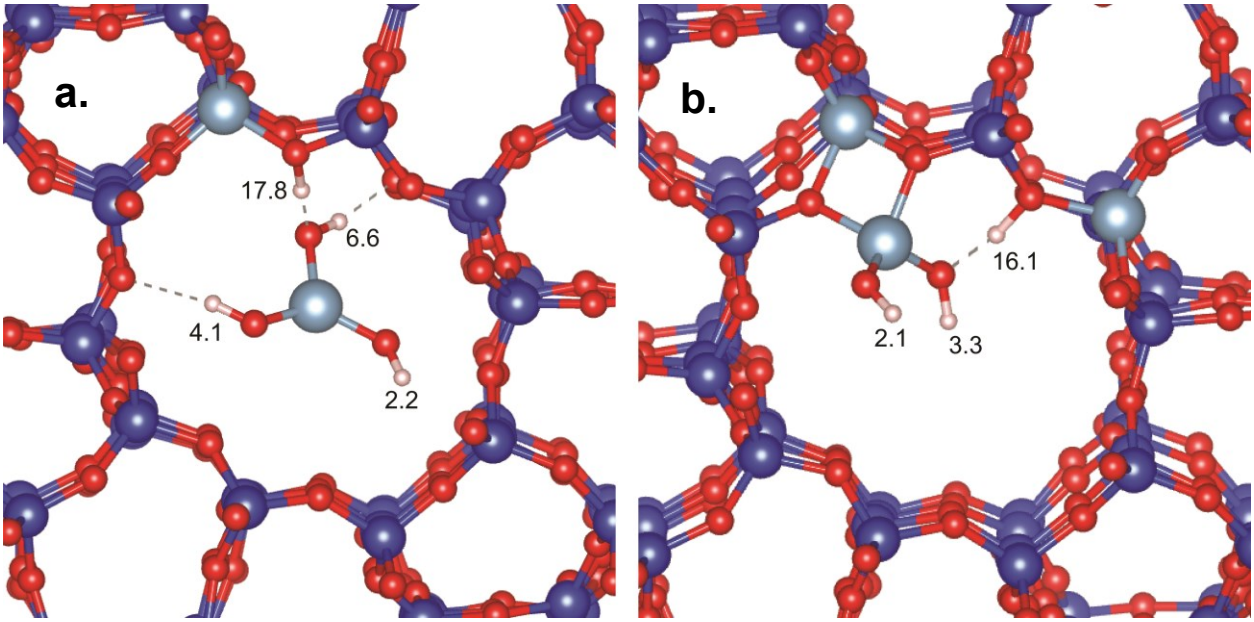

Figure 4. DFT-calculated HZSM-5 framework and extra-framework structures for **(a)** an isolated and **(b)** a paired framework acid site arising from next-nearest neighbor lattice Al atoms. The calculated ^{1}H chemical shift values are shown next to each protonic species, including the $Al(OH)_3$ and $Al(OH)_2^+$ species in (a) and (b), respectively. The calculated reference structure for an isolated BAS is shown in Figure S4.

Cation-exchange evidence for framework and non-crystalline acid sites. Combining the quantitative NMR approach described above with divalent cation titration, and using cations with differing atomic radii, provides an opportunity to probe proximate acid sites in a quantitative way and with chemical-shift resolution. An added advantage is that the NMR approach is not complicated by false-positives associated with physisorbed cations that are not proximate to active sites, as can occur in traditional UV-Vis spectrophotometric detection. Figure 5 shows the resulting spectra following exchange with Ca^{2+}, Cu^{2+}, and Ba^{2+} cations for both Si/Al = 15 (5a) and 40 (5b) catalysts, compared to the initial parent zeolite spectra. (As a control experiment, Figure S5 shows the results of exchange experiments using Na^+, clearly showing loss of essentially all signal intensity for the acid site signals in the NMR spectra, but as expected the SiOH signal is not impacted in any way.) The cationic radii increase in the order Cu^{2+}, Ca^{2+}, and Ba^{2+}, and Figure 5 shows large differences in loss of signal between Ba^{2+}, the largest of the

cations at 1.49 Å, and the two smaller cations. Cu^{2+} is commonly used for previously published work based on UV-Vis detection, and being paramagnetic could in theory induce artificial loss of signal from nearby proton spins. However, Figure 4a shows a similar response for Cu^{2+} and Ca^{2+}, which is not paramagnetic. Additionally, ^{1}H T_1 relaxation constants remain long (≥ 4 s) for both the 4.2 and 5-8 ppm species in the Cu-exchanged case, indicating that none of the remaining protons contributing to those signals are close to Cu^{2+}. There are three important conclusions from Figure 5: (1) In addition to the BAS signal, which is expected to be decrease with divalent cation titration if paired framework BASs exists, signals from the previously assigned acidic protons from EFAl/non-crystalline species (ca. 5-15 ppm) clearly respond in the same way as the BASs in 5a; (2) The overall attenuation of all assigned acidic peaks is much larger in the Si/Al=15 versus the 40 catalyst, as seen in 5a versus 5b, meaning much less uptake of divalent cations relative to total acid site number in the latter; (3) Ba^{2+} has a much larger impact relative to the smaller cations in the 15 versus the 40 catalyst. Indeed, the number of BAS's versus non-crystalline acid sites titrated in each cation exchange experiment is quantified in Table 2, and supports the points above. As expected, the SiOH peak is not impacted by exchange as proved by the constant concentration of these species in Table 2. Most importantly, all of the signals associated with non-crystalline Brønsted acid sites respond to exchange with small versus large divalent cations in the same manner as the BAS signal. For example, following Ba^{2+} titration, 22% of BAS protons remain and 20% of non-crystalline acid site protons remain. These results strongly indicate that the species are proximate and are in similar environments, i.e., inside of the zeolite channels within the ionic bonding radius of the cations, and respond similarly to their presence. If relatively small divalent cations can exchange with these proximate species, then it stands to reason that larger hydrocarbons, including the benzene and isobutane probes used here,

can similarly interact with proximate BAS and EFAl/non-crystalline acid sites simultaneously. Importantly, when a similar cation exchange experiment is performed on the Si/Al=15 catalyst whose H^+-EFAl/non-xtal sites have been reduced by AHFS washing, the reduction in total acid site signal intensity by divalent cation titration is less, as shown in Figure S6 of the Supporting Information, indicating a fewer proximate framework and defect acid sites. Exchange of a divalent cation for a single protonic site is not expected in the absence of water. Again, as stated above and shown in Figure S5, only the monovalent Na^+ cation (ionic radius = 1.02 Å) exchanges with all protonic sites in the catalyst, excluding the non-acidic SiOH signal at 2 ppm, leading to a loss of all other signals.

Table 2. Distribution of species, in units of **mmol/g**, obtained from quantitative spin-counting ^{1}H MAS NMR on the Si/Al=15 catalyst, following divalent cation exchange with the indicated cations, as shown in Figure 5.

Signal	**H^+ ZSM-5**	**Cu^{2+}-ZSM-5**	**Ca^{2+}-ZSM-5**	**Ba^{2+}-ZSM-5**
12-15 ppm	0.06	-	-	-
5-10 ppm	0.45	0.16	0.22	0.13
2.8 ppm	0.09	0.04	-	-
sum H^+ from EFAl/non-xtal (first three rows)	0.60	0.20	0.22	0.13
H^+ from BAS	0.56	0.30	0.32	0.13
SiOH	0.18	0.20	0.20	0.20

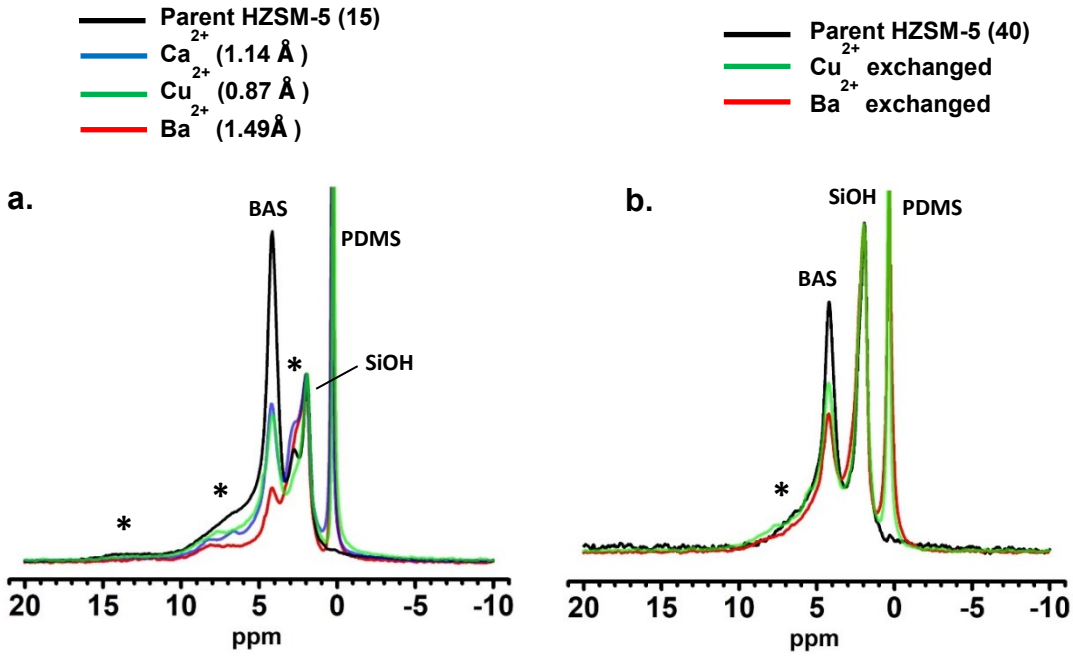

Figure 5. ^{1}H MAS NMR spectra comparing the parent HZSM-5 catalysts (black trace) for (a) Si/Al = 15 and (b) Si/Al = 40 to spectra obtained following divalent cation titrations with Ca^{2+}(blue), Cu^{2+} (green), and Ba^{2+} (red); cationic radii in angstroms (Å) are listed in parentheses in (a). The **asterisks *** denote the proton signals previously identified as arising from EFAl and non-crystalline acid sites (2.8, 5-7, and 12-15 ppm). As in previous figures, PDMS is the added intensity standard. For reference, Figure S5 shows results of control experiments involving Na^{+} titrations in which all signals except the non-acidic SiOH signal are eliminated.

As discussed above and in a previous communication,[15] the 12-15 ppm and 2.8 ppm species are removed by AHFS washing at room temperature without reduction of the framework BAS concentration, and are thus assigned to species arising from extra-framework aluminol species, or their interaction with crystalline BASs as shown in Figure 4.[32] However, multiple experimental runs show that ca. 35-40% of the species giving rise to the 5-10 ppm peak can be removed by washing without perturbing the crystalline framework, even though the data in Table 2 shows that over 70% of the species giving rise to this peak can be exchanged by Ba^{2+}. Figure 6a shows that at least two components are required to fit the total intensity in the 5-7 ppm region of the spectrum, as indicated by the green peaks. Figure 6a shows components obtained from the complete fitting (red trace) of the experimental data (black trace), with the deconvoluted

component from the large BAS peak (4-5 ppm) omitted for clarity in 6a and 6b, and the large isobutane methyl peak component omitted for clarity in 6b. The spectrum in 6b was obtained following adsorption of 1 equivalent of isobutane-d_{10} on the same type of Si/Al = 15 catalyst shown in 6a, after ca. 5 minutes of H/D exchange. The catalyst in 6b is a different catalyst dehydration preparation than that in 6a, but from the same master batch as that from which the catalyst in 6a was prepared. Previously, shifts of the framework BAS signal at 4.2 ppm have been reported and discussed in the literature as indicative of adsorption complex formation.[57] The dashed diagonal lines show that the two components that comprise the broad 5-7 ppm signal experience a 1-1.5 ppm downfield shift following isobutane adsorption, from 5.1 to 7.0 and 6.8 to 8.3 ppm, respectively, reported here for the first time. The magnitude of this shift is similar to the ca. 1-ppm downfield shift of the BAS after isobutane adsorption. This induced shift rules out their previous assignment as strongly adsorbed water clusters or residual ammonia, since it would not be reasonable for isobutane molecules to displace molecules with larger proton affinities or to deshield them, given the nonpolar nature of isobutane. The solid line shows the SiOH peak as constant, both in position and intensity, consistent with its non-acidic nature. The 5-7 ppm components in 6b exhibit significantly reduced signal area, indicating their reactivity with isobutane-d_{10}. Comparing the intensity loss of the two 5-7 ppm components to the BAS signal indicates that they are at least as reactive as the BAS, if not more reactive. Recall, following AHFS-washing under mild conditions, Table 1 and Figure 1 showed that ca. 35-40% of the species giving rise to signal intensity in the 5-7 ppm region are eliminated along with all of the other H-EFAl species. Importantly, catalyst reactivity decreased dramatically in Figure 3, indicating that the initial HZSM-5 catalyst has a complex distribution of acidic protons giving rise to the signals in this region, which along with the other H-EFAl species render the catalyst

most active. Moreover, to assign the remaining intensity in the 5-7 ppm region after AHFS washing to hydrogen-bonded framework BASs, consistent with earlier proposals in the literature, would suggest those species with intensity remaining in the 5-7 ppm region are less reactive in the hydrocarbon exchange reactions, as per Figure 3 and Table 1. It is important to recall that the AHFS-washed sample still has the same framework BAS site density as the parent HZSM-5. It is certainly possible that some framework BAS's contribute to the amount of signal in the 5-7 ppm region that is lost following AHFS removal, as they are likely more susceptible given their increased reactivity, and as supported by a constant BAS 4.2 ppm signal in the ^{1}H spectrum, but a difference in the total [BAS] measured by that signal and the IPA TPD. In total, these data suggest that ***both BASs and acidic protons from EFAl and non-crystalline, i.e., defect sites*** must be present for maximum catalyst reactivity. Previously published data show that on timescales much longer than the 5-minute reaction time in 6b, all signals in the HZSM-5 spectra except the SiOH signal at 2 ppm undergo isotopic exchange with either isobutane-d_{10} or D_2O at room temperature, resulting in essentially complete intensity loss of the 2.8, 4.2, 5-7, and 12-15 ppm peaks and indicating that their associated acid site species are accessible.[15]

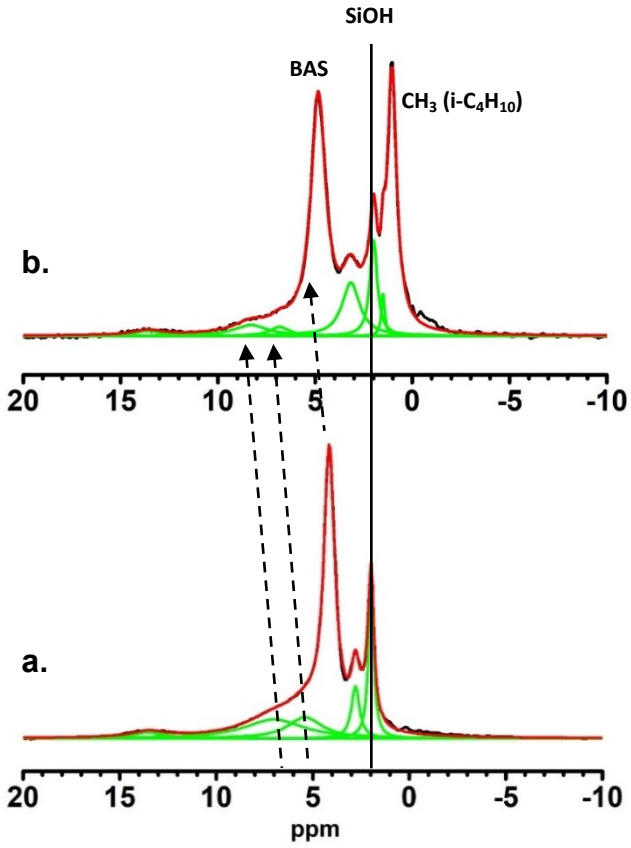

Figure 6. (a) ^{1}H MAS NMR spectrum comparing the dry parent Si/Al = 15 HZSM-5 catalyst (black trace) to its total fit using the species described in the text (red trace). The spectrum in **(b)** was obtained following adsorption of 1 molecule of isobutane-d_{10} per total acidic proton site (i.e., 1.1 mmol/g) on the same catalyst, showing the large isobutane CH_3 signal at 1 ppm and a very small CH signal near 1.4 ppm, after ca. 5 minutes of H/D exchange with the protonated zeolite.

Brønsted sites and synergies with H_2O. Water present in either vapor or liquid phases can dramatically impact zeolite chemistries, ranging from unexpected increases in reactivity[58] to deleterious impacts on framework stability.[59] Recent reports of increases in reaction rate for room-temperature reaction rates in HZSM-5 in the presence of small amounts of water are not mechanistically well-understood.[60-62] Figure 7 indicates that proximate framework and defect Brønsted sites can play a significant role in water synergies. Figure 7 shows a series of in-situ ^{1}H MAS NMR spectra acquired after adsorbing isobutane-d_{10} on the AHFS-washed HZSM-5

Si/Al=15 sample, thereby removing the majority of extra-framework Brønsted sites, and which also contains co-adsorbed water at low loadings, i.e., < 0.1 equivalent per acid site. Table 1 indicates that this catalyst has the lowest amount of EFAl- and non-crystalline Brønsted sites among the Si/Al=15 samples. Time-dependent analysis of the isobutane CH_3 peak intensity in the same manner as described above for benzene (Figure 3) yields an H/D exchange rate constant of 2×10^{-6} s^{-1}, which is the lowest rate constant measured for any of the Si/Al=15 samples, and similar to that of the initial Si/Al=40 catalyst/isobutane data discussed in Figure 1e above. Previously published works show that water can significantly increase reaction rates for as-prepared/as-received HZSM-5 at Si/Al = 15.[37,62] Importantly, even for this low reactivity catalyst, Figure 7 shows that water is involved in H/D exchange with isobutane due to the time-dependent H_2O-signal decrease. With time, BAS and H_2O signal intensities markedly decrease and isobutane CH_3 signals increase. If water can actively participate in the exchange mechanism for an AHFS-washed catalyst that exhibits a much smaller reaction rate than the parent HZSM-5 catalyst, and where the defect Brønsted site concentration is very low, then a systematic interrogation of the role of water in any as-synthesized HZSM-5 catalyst must include consideration of the framework/defect site Brønsted-Brønsted synergies identified above. As additional evidence, Figure S7 in the Supporting Information provides experimental verification that all catalyst protons except the SiOH protons undergo H/D exchange with isobutane at room temperature even in the absence of water, resulting in essentially complete intensity loss of the 2.8, 4.2, 5-7, and 12-15 ppm peaks and indicating that their associated protonic species are both acidic and accessible.

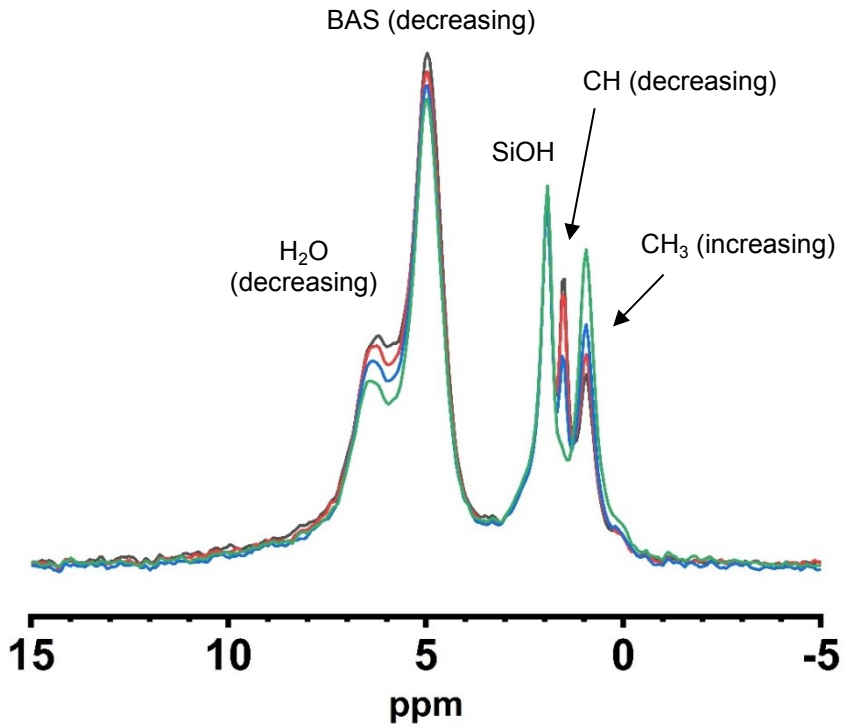

Figure 7. In-situ ^{1}H MAS NMR data following adsorption of isobutane-d_{10} on washed HZSM-5 catalyst that contains added water, for reaction times ranging from a few minutes (black trace) to ca. 20 hours (green trace), with red and blue traces for intermediate times. Peak amplitudes versus time are denoted as "increasing" or "decreasing", as appropriate for that species.

Clarifying isobutane/HZSM-5 exchange mechanism. The reaction rate for the system in Figure 7 is at least two orders of magnitude smaller (10^{-6} s^{-1}) compared to previously published isobutane/HZSM-5 systems (10^{-4} s^{-1}),[63-66] yielding a resolved isobutane CH signal at 1.6 ppm for the first time as labeled in the figure. The experimental detection of H/D exchange at the CH position helps clarify long-standing questions about whether or not the mechanism for isobutane-zeolite H/D exchange includes the methine proton, or proceeds only via the methyl group.[63-66] The one-dimensional in-situ spectra in Figure 7 show that the CH proton participates in H/D

exchange with the BAS and water in this case, in addition to the exchange previously reported for the CH_3 groups. The much larger reaction rate on the as-received catalyst, which is the same catalyst used in prior reports in which CH exchange was not observed, makes detection of the 1.6 ppm CH peak even at the first time point difficult, as seen by the weak and poorly resolved 1.6 ppm CH signal (appearing as downfield shoulder on the CH_3 signal) in the spectrum in Figure 6b above. This new experimental result is in agreement with recent work by Sauer, in which detailed quantum chemical calculations indicate that the direct methyl protonation pathway is not operative in the isobutane/HZSM-5 system.[67] Figure S7 in the Supporting Information provides additional experimental verification that all catalyst protons except the SiOH protons undergo H/D exchange with isobutane at room temperature even in the absence of water, as all catalyst proton signals are significantly attenuated after reaction.

Brønsted-Lewis versus Brønsted-Brønsted synergy. In the past, multiple studies have pointed to the possibility of enhanced Brønsted acidity from nearby Lewis sites, e.g., EFAl species, and strong evidence to support this contribution exists.[68,69] Other recent studies have called their contributions into question, or emphasized the importance of Brønsted-Brønsted synergies between framework BASs.[70-73] We recognize that Brønsted-Lewis contributions could be active in some of the catalysts described in this work, and do not exclude them as a potentially important contributor. However, the data presented above and in the Supporting information show that (1) all protonic species except SiOH, including those from these non-BAS sources, undergo reaction; (2) first-principles calculations support their acidic nature, based on agreement between DFT and the significant downfield proton chemical shifts (5-15 ppm) observed experimentally; (3) all protonic species, excluding SiOH, exhibit adsorbate-induced downfield shifts from non-polar isobutane probe molecules. That such reactivity enhancements involving

proton transfer involve all of the species arising from non-BAS protons in room-temperature reactions suggest that they cannot be ignored in high-temperature processes typical of those zeolite catalysis. Moreover, the generation of these species in the Si/Al=40 catalysts and concimitant reactivity changes (Figure 1e and surrounding discussion) indicates that this is unique from the framework Brønsted-Brønsted synergies, since the mild steaming only leads to a decrease in BAS concentration. Our experimental data, theory calculations, and proposed synergistic effects are in agreement with previously published work by Bhering and Mota, in which their calculations indicated that hydrogen bonding between extra-framework aluminols and the BAS lead to increased acidity, not Brønsted-Lewis synergy.[70,71] Further, both Hunger and Bruno have discussed that Brønsted character could potentially be assigned to non-framework aluminol species.[74,75] In total the Brønsted-Brønsted contributions discussed here cannot be excluded as relevant contributions to catalyst reactivity, but that their relative contributions are likely more significant at low or mild temperatures versus in the several hundred degree temperature range associated with gas-phase cracking or isomerization reactions. Future work is needed to clarify this issue, with a particular focus on the role that hydrated vs. dehydrated alumina species proximate to framework BASs play in different reaction types at different temperatures, with and without the presence of water.

Conclusions

Brønsted-Brønsted synergies between framework bridging acid sites and extra-framework/non-crystalline acidic proton sites are operative in high-Al content HZSM-5, and lead to increased reactivity relative to catalysts with identical framework acid densities. Combined spectroscopic, reactivity, theory, and post-synthetic treatments indicated that paired-Brønsted

acid sites in the framework contribute less to overall catalyst activity in room-temperature probe reactions than do proximate framework and non-framework/non-crystalline Brønsted sites. Reaction rates for several experiments involving Si/Al = 15 and 40 HZSM-5 catalysts indicated that the rate does not correlate well with framework BAS concentration, but depends more on the concentration of proximate Brønsted acid sites arising from non-framework and non-crystalline sites. Brønsted-Brønsted synergies do not preclude Brønsted-Lewis synergies arising from EFAl species, but the fact that protons from EFAl species are also active means that the overall catalyst acidity is more complex than a BAS activated by a proximate non-framework Al atom, and that mechanistic proposals must be understood in the context of Brønsted acid site distributions. As an initial example, selectively modifying the distribution of acid site species enabled detection of H/D exchange and the CH position of isobutane for the first time, helping to clarify mechanistic uncertainties surrounding its reactivity in HZSM-5. Future work will be needed to determine the relative role of this contribution at higher-reaction temperatures, and in the presence versus the absence of water.

Supporting Information. Additional characterization data including x-ray, elemental, and NMR results are provided and available free of charge via the Internet at http://pubs.acs.org.

Acknowledgements. This material is based upon work supported by the National Science Foundation under Grant No. CHE-1764116, and is gratefully acknowledged. Instrumentation support for the solid-state NMR system was provided in part through the Oklahoma State University Core Facilities program.

References

(1) Corma, A. Inorganic Solid Acids and Their Use in Acid-Catalyzed Hydrocarbon Reactions. *Chem. Rev.* **1995**, *95*, 559-614.

(2) Thomas, J. M.; Thomas, W. J. *Principles and Practice of Heterogeneous Catalysis*, First Edition, VCH Publishing, **2005,** Weinheim, Germany.

(3) Derouane, E. G.; Védrine, J. C.; Pinto, R. R.; Borges, P. M.; Costa, L.; Lemos, M. A. N. D. A.; Lemos, F.; Ribeiro, F. R. The Acidity of Zeolites: Concepts, Measurements, and Relations to Catalysis. *Catal. Rev.* **2013**, *55*, 454-515.

(4) Cheng, Y.-T.; Jae, J.; Shi, J.; Fan, W.; Huber, G. W. Production of Renewable Aromatic Compounds by Catalytic Fast Pyrolysis of Lignocellulosic Biomass with Bifunctional Ga/ZSM-5 Catalysts. *Angew. Chem. Int. Ed. Eng.* **2012**, *51*, 1387-1390.

(5) Ennaert, T.; Van Aelst, J.; Dijkmans, J.; De Clercq, R.; Schutyser, W.; Dusselier, M.; Verboekend, D.; Sels, B. F. Potential and Challenges of Zeolite Chemistry in the Catalytic Conversion of Biomass. *Chem. Soc. Rev.* **2016**, *45*, 584-611.

(6) Zapata, P. A.; Faria, J.; Ruiz, M. P.; Jentoft, R. E.; Resasco, D. E. Hydrophobic Zeolites for Biofuel Upgrading Reactions at the Liquid-Liquid Interface in Water/Oil Emulsions. *J. Am. Chem. Soc.* **2012**, *134*, 8570-8578.

(7) Pagan-Torres, Y.; Wang, T.; Gallo, J. M. R.; Shanks, B. H.; Dumesic, J. A. Production of 5-Hydroxymethyfurfural from Glucose Using a Combination of Lewis and Brønsted Acid Catalysts in Water in a Biphasic Reactor. *ACS Catal.* **2012**, *2*, 930-934.

(8) Lehman, S. F.; Larsen, S. C. Zeolite and Mesoporous Silica Nanomaterials: Greener Syntheses, Environmenta Applications, and Biological Toxicity. *Environ. Sci. Nano* **2014**, *1*, 200-213.

(9) Misaelides, P. Application of Natural Zeolites in Environmental Remediation. *Micropor. Mesopor. Mater.* **2011**, *144*, 15-18.

(10) Kabalan, I.; Lebeau, B.; Nouali, H.; Toufaily, J.; Hamieh, T.; Koubaissy, B.; Bellat, J. P.; Daou, T. J. New Generation of Zeolite Materials for Environmental Applications. *J. Phys. Chem. C* **2016**, *120*, 2688-2697.

(11) Boudart, M. Turnover Rates in Heterogeneous Catalysis. *Chem. Rev.* **1995**, *95*, 661-666.

(12) Haag, W. O.; Lago, R. M.; Weisz, P. B., The Active Site of Acidic Aluminosilicate Catalysts. *Nature* **1984**, *309*, 589-591.

(13) Knott, B. C.; Nimlos, C. T.; Robichaud, D. J.; Nimlos, M. R.; Kim, S.; Gounder, R., Consideration of the Aluminum Distribution in Zeolites in Theoretical and Experimental Catalysis. *ACS Catal.* **2018**, *8*, 770-784.

(14) Perras, F. A.; Wang, Z.; Naik, P.; Slowing, I.; Pruski, M., Natural Abundance ^{17}O DNP NMR Provides Precise O-H Distances and Insights into Brønsted Acidity of Heterogeneous Catalysts. *Angew. Chem. Int. Ed.* **2017**, *56*, 9165-9169.

(15) Chen, K.; Abdolrhamani, M.; Sheets, E.; Freeman, J.; Ward, G.; White, J. L., Direct Detection Of Multiple Acidic Sites in Zeolite HZSM-5**.** *J. Am. Chem. Soc.* **2017,** *139*, 18698-18704.

(16) Janda, J.; Bell, A. T.; Effects of Si/Al Ratio on the Distribution of Framework Al and on the Rates of Alkane Monomolecular Cracking and Dehydrogenation in H‑MFI. *J. Am. Chem. Soc.* **2013**, *135*, 19193−19207.

(17) Jones, A. J.; Carr, R. T.; Zones, S. I.; Iglesia, E., Acid Strength and Solvation in Catalysis by MFI Zeolites and Effects of the Identity, Concentration, and Location of Framework Heteroatoms. *J. Catal.* **2014**, *312*, 58-68.

(18) Schallmoser, S.; Ikuno, T.; Wagenhofer, M. F.; Kolvenbach, R.; Haller, G. L.; Sanchez-Sanchez, M.; Lercher, J. A., Impact of the Local Environment of Brønsted Acid Sites in HZSM-5 on the Catalytic Activity in n-Pentane Cracking. *J. Catal.* **2014**, *316*, 93-102.

(19) Dedecek, J.; Sobalik, Z.; Wichterlova, B., Siting and Distribution of Framework Aluminum Atoms in Silicon-Rich Zeolites and Impact on Catalysis. *Cat. Rev. Sci. Eng.* **2012**, *54*, 135-223.

(20) Li, C.; Vidal-Moya, A.; Miguel, P. J.; Dedecek, J.; Boronat, M.; Corma, A., Selective Introduction of Acid Sites in Different Confined Positions in ZSM-5 and Its Catalytic Implications. *ACS Catal.* **2018**, *8*, 7688-7697.

(21) Di Iorio, J. R.; Gounder, R., Controlling the Isolation and Pairing of Aluminum in Chabazite Zeolites Using Mixtures of Organic and Inorganic Structure-Directing Agents. *Chem. Mater.* **2016**, *28*, 2236-2247.

(22) Liang, T.; Chen, J.; Qin, Z.; Li, J.; Wang, P.; Wang, S.; Wang, G.; Dong, M.; Fan, W.; Wang, J., Conversion of Methanol to Olefins over HZSM-5 Zeolite: Reaction Pathway is Related to Framework Aluminum Siting. *ACS Catal.* **2016**, *6*, 7311-7325.

(23) Song, C.; Chu, Y.; Wang, M.; Shi, H.; Zhao, L.; Guo, X.; Yang, W.; Shen, J.; Xue, N.; Peng, L.; Ding, W., Cooperativity of Adjacent Brønsted Sites in MFI Zeolite Channel Leads to Enhanced Polarization and Cracking of Alkanes. *J. Catal.* **2017**, *349*, 163-174.

(24) Yang, C.; Janda, A.; Bell, A. T.; Lin, L., Atomistic Investigations of the Effects of Si/Al Ratio and Al Distribution on the Adsorption Selectivity of n-Alkanes in Brønsted-Acid Zeolites. *J. Phys. Chem. C.* **2018**, *122*, 9397-9410.

(25) Paolucci, C.; Parekh, A.; Khurana, I.; Iorio, J.; Li, H.; Caballero, J.; Shih, A.; Anggara, T.; Delgass, W. N.; Miller, J. T.; Ribeiro, F. H.; Gounder, R.; Schneider, W. F., Catalysis

in a Cage: Condition-Dependent Speciation and Dynamics of Exchanged Cu Cations in SSZ-13 Zeolites. *J. Am. Chem. Soc.* **2016**, *138*, 6028-6048.

(26) Abdolrahmani, M.; Chen, K.; White, J. L., Assessment, Control, and Impact of Brønsted Acid Site Heterogeneity in Zeolite HZSM-5. *J. Phys. Chem. C* **2018**, *122*, 15520-15528.

(27) Pashkova, V.; Sklenak, S.; Klein, P.; Urbanova, M.; Dedecek, J., Location of Framework Al Atoms in the Channels of ZSM-5: Effect of the (Hydrothermal) Synthesis. *Chem. Eur. J.* **2016**, *22*, 3937-3941.

(28) Holzinger, J.; Beato, P.; Lundegaard, L.; Skibsted, J., Distribution of Aluminum over the Tetrahedral Sites in ZSM-5 Zeolites and Their Evolution after Steam Treatment. *J. Phys. Chem. C* **2018**, *122*, 15595-15613.

(29) Dib, E.; Mineva, T.; Veron, E.; Sarou-Kanian, V.; Fayon, F.; Alonso, B., ZSM-5 Zeolite: Complete Al Bond Connectivity and Implications on Structure Formation from Solid-State NMR and Quantum Chemistry Calculations. *J. Phys. Chem. Lett.* **2018**, *9*, 19-24.

(30) Xue, N.; Vjunov, A.; Schallmoser, S.; Fulton, J.; Sanchez-Sanchez, M.; Hu, J.; Mei, D.; Lercher, J. A., Hydrolysis of Zeolite Framework Aluminum and its Impact on Acid Catalyzed Alkane Reactions. *J. Catal.* **2018**, *365*, 359-366.

(31) Wang, Z.; Jiang, Y.; Lafon, O.; Trebosc, J.; Kim, K. D.; Stampfl, C.; Baiker, A.; Amoureaux, J. P.; Huang, J., Brønsted Acid Species Based on Penta-Coordinated Aluminum Species. *Nature Comm.* **2016**, *7*, 13820-13824.

(32) Yu, Z.; Li, S.; Wang, Q.; Zheng, A.; Jun, X.; Chen, L.; Deng, F., Brønsted-Lewis Acid Synergy in HZSM-5 and H-MOR Zeolites Studied by ^{1}H and ^{27}Al DQ-MAS NMR. *J. Phys. Chem. C* **2011**, *115*, 22320-22327.

(33) Martínez, A.; López, C., The Influence of ZSM-5 Composition and Crystal Size on the In-situ conversion of Fischer-Tropsch Products over Hybrid Catalysts. *Applied Catalysis A: General* **2005**, *294*, 251-259.

(34) Garralon, G.; Fornes, V.; Corma, A., Faujasites Dealuminated with Ammonium Hexafluroosilicate. *Zeolites* **1988**, *8*, 268-272.

(35) Breck, D. W.; Blass, H.; Skeels, G. W. *U. S. Pat.4503023*, **1985**.

(36) Munson, E. J.; Ferguson, D. B.; Kheir, A. A.; Haw, J. F., Applications of a New CAVERN Design to the Study of Reactions on Catalysts using In-Situ Solid-State NMR. *J. Catal.* **1992**, *136*, 504-509.

(37) Chen, K.; Gumidyala, A.; Abdolrhamani, M.; Villines, C.; Crossley, S.; White, J. L., Trace Water Amounts can Increase Benzene H/D Exchange Rates in an Acidic Zeolite. *J. Catal.* **2017,** *351*, 130-135.

(38) Cory, D. G.; Ritchey, W. M., Suppression of Signals from the Probe in NMR T_1 Measurements. *Spectrosc. Lett.* **1988**, *21*, 551-558.

(39) Kresse, G.; Joubert, D. From ultrasoft pseudopotentials to the projector augmented-wave method. *Phys Rev B* **1999**, *59*, 1758-1775.

(40) Blochl, P. E. Projector Augmented-Wave Method. *Phys Rev B* **1994**, *50*, 17953-17979.

(41) Perdew, J. P.; Ernzerhof, M. Generalized gradient approximation made simple. *Phys. Rev. Lett.* **1996**, *77*, 3865–3868.

(42) Grimme, S.; Antony, J.; Ehrlich, S.; Krieg, H. A consistent and accurate ab initio parametrization of density functional dispersion correction (DFT-D) for the 94 elements H-Pu. *J. Chem. Phys.* **2010**, *132*, 154104.

(43) Grimme, S.; Ehrlich, S.; Goerigk, L. Effect of the damping function in dispersion corrected density functional theory. *J. Comput. Chem.* **2011**, *32*, 1456-1465.

(44) Koningsveld, H. v. High-temperature (350 K) orthorhombic framework structure of zeolite H-Zsm-5. *Acta Crystallogr. B* **1990**, *46*, 731–735.

(45) Ghorbanpour, A.; Rimer, J. D.; Grabow, L. C. Periodic, vdW-corrected density functional theory investigation of the effect of Al siting in H-ZSM-5 on chemisorption properties and site-specific acidity. *Catalysis Communications* **2014**, *52*, 98-102.

(46) Zeets, M.; Resasco, D. E.; Wang, B. Enhanced chemical activity and wettability at adjacent Bronsted acid sites in HZSM-5. *Catalysis Today* **2018**, *312*, 44-50.

(47) Pickard, C. J.; Mauri, F. All-electron magnetic response with pseudopotentials: NMR chemical shifts. *Phys Rev B* **2001**, *63*, 245101.

(48) Yates, J. R.; Pickard, C. J.; Mauri, F. Calculation of NMR chemical shifts for extended systems using ultrasoft pseudopotentials. *Phys Rev B* **2007**, *76*, 024401.

(49) Hunger, M., Multinuclear Solid-State NMR Studies of Acidic and Non-Acidic Hydroxyl Protons in Zeolites. *Solid State Nucl. Magn. Reson.* **1996**, *6*, 1-29.

(50) Brunner, E.; Ernst, H.; Freude, D.; Hunger, M.; Krause, C. B.; Prager, D.; Reschetilowski, W.; Schwieger, W.; Bergk, ^{1}H Solid-State NMR and Catalytic Studies of Mildly Dealuminate HZSM-5. K. H. *Zeolites* **1989**, *9*, 282-286.

(51) Batamack, P.; Doremieux-Morin, C.; Fraissard, J.; Freude, D., Broad-Line and High-Resolution NMR Studies Concerning the Hydroxonium Ion in HZSM-5 Zeolites. *J. Phys. Chem.* **1991**, *95*, 3790-3796.

(52) Gabrienko, A. A.; Danilova, I.; Arzumanov, S.; Pirutko, L.; Freude, D.; Stepanov, A. G., Direct Measurement of Zeolite Acidity by FTIR Spectroscopy: Solid-State ^{1}H MAS

NMR Approach for Reliable Determination of Intergrated Molar Absorption Coefficients. *J. Phys. Chem. C.* **2018**, *122*, 25386-25395.

(53) Beck, L. W.; White, J. L.; Haw, J. F., ^{1}H-^{27}Al Double-Resonance Experiments in Solids: An Unexpected Observation in the ^{1}H MAS Spectrum of HZSM-5. *J. Am. Chem. Soc.* **1994**, *116*, 9657-9661.

(54) Huo, H.; Peng, L.; Grey, C. P., Low Temperature ^{1}H MAS NMR Spectroscopy Studies of Proton Motion in Zeolite HZSM-5. *J. Phys. Chem. C* **2009**, *113*, 8211-8219.

(55) Wang, X.; Coleman, J.; Jia, X.; White, J. L., Quantitative Investigations of Transient Acidity in Zeolites and Molecular Sieves, *J. Phys. Chem. B.* **2002**, *106*, 4941-4946.

(56) Wang, C.; Mao, X.; Caratzoulas, S.; Gorte, R. J., H-D Exchange of Simple Aromatics as a Measure of Brønsted-Acid Site Strengths in Solids. *Catal. Lett.* **2018**, *148*, 3548-3556.

(57) Truitt, M.; Toporek, S.; Rivera, R.; White, J. L., Identification of an Adsorption Complex between and Alkane and Zeolite Active Sites. *J. Am. Chem. Soc.* **2004**, *126*, 11144-11145.

(58) Xue, N.; Vjunov, A.; Schallmoser, S.; Fulton, J.; Sanchez-Sanchez, M; Hu, J. Z.; Mei, D.; Lercher, J. A., Hydrolysis of Zeolite Framework Aluminum and its Impact on Acid Catalyzed Alkane Reactions. *J. Catal.* **2018,** *365*,359-366.

(59) Zhang, L.; Chen, K.; Chen, B.; White, J. L.; Resasco, D. E., Factors that Determine Zeolite Stability in Hot Liquid Water. *J. Amer.Chem. Soc.* **2015,** *137*, 11810-11819.

(60) Yoon, J. S.; Choi, J. W.; Suh, D. J.; Lee, K.; Lee, H.; Ha, J. M. Water-Assisted Selective Hydrodeoxygenation of Lignin-Derived Guaiacol to Monooxygenates. *ChemCatChem* 2015, *7*, 2669-2674.

(61) Motokura, K. ; Matsunaga, S.; Noda, H. ; Miyaji, A. ; Baba, T. Water-Accelerated Allylsilylation of Alkenes Using a Proton-Exchanged Montmorillonite Catalyst. *ACS Catal.* **2012**, 2, 1942-1946.

(62) Chen, K.; Damron, J.; Pearson, C.; Resasco, D.; Zhang, L.; White, J. L. Zeolite Catalysis: Water Can Dramatically Increase or Suppress Alkane C-H Bond Activation. *ACS Catal.* **2014,** *4,* 3039-3044.

(63) (a) Haouas, M. ; Walspurger, S. ; Sommer, J., *J. Am. Chem. Soc.* **2004**, 126, 599. (b) Sommer, J.; Habermacher, D.; Jost, R.; Sassi, A.; Stepanov, A. G.; Luzgin, M. V.; Freude, D.; Ernst, H.; Martens, J. *J. Catal.* **1999***, 181*, 265.

(64) Walspurger, S. ; Sun, Y.; Sido, A. S. ; Sommer, J. , *J. Phys. Chem. B* **2006**, 110, 18368.

(65) Truitt, M. J.; Rovira, R.; White, J. L. *J. Am. Chem. Soc.* **2006**, *128*, 1847-1852.

(66) Sido, A. S. S.; Walspurger, S.; Barbiche, J.; Sommer, J., Low-Temperature Alkane C-H Bond Activiation by Zeolites. *Chem. Eur. J.* **2010**, *16*, 9034-9039.

(67) Rybicki, M.; Sauer, J. Ab Initio Prediction of Proton Exchange Barriers for Alkanes at Brønsted Sites of Zeolite H‑MFI. *J. Am. Chem. Soc.* **2018**, *140*, 18151-18161.

(68) Lago, R. M.; Haag, W. O.; Mikovsky, R. J.; Olson, D. H.; Hellring, S. D.; Schmitt, K. D.; Kerr, G. T., The Nature of Catalytic Sites in HZSM-5: Activity Enhancement. *Stud. Surf. Sci. Catal.* **1986**, *28*, 677-684.

(69) Fritz, P. O.; Lunsford, J. H., The Effect of Sodium Poisoning on Dealuminated Y-Type Zeolites, *J. Catal.* **1989**, *118*, 85-98.

(70) Mota, C. J.; Bhering, D. L.; Rosenbach, N., A DFT Study of the Acidity of Ultrastable Y Zeolite: Where is the Brønsted/Lewis Acid Synergism? *Angew. Chem. Int. Ed.* **2004**, *43*, 3050-3053.

(71) Bhering, D. L.; Ramirez-Solis, A.; Mota, C. J., A Density Functional Theory Approach to Extraframework Aluminum Species in Zeolites. *J. Phys. Chem.B* **2003**, *107,*4342-4347.

(72) Nystrom, S.; Hoffman, A.; Hibbits, D., Tuning Brønsted Acid Strength by Altering Site Proximity in CHA Framework Zeolites. *ACS Cat*al. **2018**, *8*, 7842-7860.

(73) Bernauer, M.; Tabor, E.; Pashkova, V.; Kaucky, D.; Sobalik, Z.; Wichterlova, B.; Dedecek, J., Proton Proximity- New Key Parameter Controlling Adsorption, Desorption, and Activity in Propene Oligomerization of HZSM-5 Zeolites. *J. Catal.* **2016**, *344*, 157-172.

(74) Hunger, M.; Freude, D.; Bremer, H.; Jank, M.; Wendlandt, K. P., High-Resolution Proton Magnetic Resonance and Catalytic Studies Concerning Brønsted Centers in Amorphous Al_2O_3-SiO_2 Solids. *Chem. Phys. Lett.* **1983**, *100*, 29-33.

(75) DeCanio, E. C.; Edwards, J. C.; Bruno, J. W., Solid-State ^{1}H MAS NMR Characterization of γ-Alumina and Modified γ-Aluminas. *J. Catal.* **1994**, *148*, 76-83.

TOC Figure: